J. Fluid Mech. (2005), *vol.* 539, *pp.* 417–443. © 2005 Cambridge University Press
doi:10.1017/S0022112005005707 Printed in the United Kingdom

A hydroelastic model of hydrocephalus

By ALAN SMILLIE[1]†, IAN SOBEY[1]‡ AND ZOLTAN MOLNAR[2]

[1]Computing Laboratory, Wolfson Building, Parks Road, Oxford OX1 3QD, UK
[2]Department of Human Anatomy, South Parks Road, Oxford OX1 3QX, UK

(Received 11 February 2004 and in revised form 13 April 2005)

We combine elements of poroelasticity and of fluid mechanics to construct a mathematical model of the human brain and ventricular system. The model is used to study hydrocephalus, a pathological condition in which the normal flow of the cerebrospinal fluid is disturbed, causing the brain to become deformed. Our model extends recent work in this area by including flow through the aqueduct, by incorporating boundary conditions that we believe accurately represent the anatomy of the brain and by including time dependence. This enables us to construct a quantitative model of the onset, development and treatment of this condition. We formulate and solve the governing equations and boundary conditions for this model and give results that are relevant to clinical observations.

1. Introduction

Hydrocephalus is an illness in which abnormal flow of cerebrospinal fluid (CSF) through the cerebral ventricular system causes the brain to become deformed. The disease itself is well known, owing both to its relatively high incidence and to its debilitating and often fatal effects (Drake & Sainte-Rose 1995). Despite the level of awareness and the progress that has been made in recent decades in understanding the condition, a treatment that is both reliable and widely applicable remains elusive, see Drake, Kestle & Milner (1998).

CSF is produced mainly in the choroid plexuses; long, convoluted strands of vascularized tissue located in the lateral, third and fourth ventricles. The mechanism by which fluid is produced and secreted is complex, but the production rate of around 500 ml/day in human adults is well known and is reported to be independent of external influences such as intraventricular pressure (Bradbury 1993). Given that the total volume of the cerebral ventricular system is around 150 ml, then the CSF is renewed several times daily (Nolte 2002, p. 105).

In a healthy brain, CSF flows from production sites in the choroid plexuses of the lateral and third ventricles through a single narrow cerebral aqueduct and into a fourth ventricle. It then moves through another series of narrow passageways known as the median and lateral apertures into the pontine cistern and cisterna magna near the base of the skull, from where it passes into the subarachnoid space between the brain and the dura mater. Fluid also flows in the subarachnoid space around the spinal cord.

† Present address: Imperial College, London 5W7 2AZ, UK.
‡ Author to whom correspondence should be addressed.

https://doi.org/10.1017/S0022112005005707 Published online by Cambridge University Press

CSF absorption occurs in the arachnoid villi, small granulations of the arachnoid that protrude into the dura mater. The barrier between the CSF and the blood in these granulations is thin, enabling CSF to pass into the bloodstream where it is absorbed. In contrast with CSF production, the rate of absorption is pressure dependent, specifically depending upon the difference between the intraventricular pressure and the superior sagittal venous pressure (Albeck *et al.* 1991; Bradbury 1993). The structure of the arachnoid villi is such that even in the unlikely event of venous blood pressure exceeding the intraventricular pressure, no flow will take place from the blood into the CSF system, so that the villi effectively act as a one-way valve for removal of CSF.

The build-up of fluid associated with hydrocephalus may in theory be caused by overproduction of CSF in the ventricles, under-absorption in the subarachnoid space or some obstruction of the CSF pathways. With the exception of a few rare cases, it is the latter of these that is the cause of the illness.

Obstruction of the CSF pathways can happen at any point in the ventricular system, but the long narrow aqueduct of Sylvius that runs between the third and fourth ventricles is reported as being the most frequent site for a blockage to occur (Weller, Kida & Harding 1993). The potential causes of a blockage in the flow pathways are many and varied. The most frequent cause of congenital and infantile hydrocephalus is a malformation in one or more parts of the ventricular system, for example stenosis of the aqueduct or membranous occlusion of the foramen of Monro. A blockage can also be the result of a blood clot entering the CSF system and blocking the aqueduct.

A consequence of the disease is normally oedema of the parenchyma, particularly the white matter adjacent to the ventricles. It is this oedema, together with the deformation of the brain itself that is the cause of most of the long-term tissue damage associated with hydrocephalus, which can result in a range of symptoms including headaches, intellectual impairment and ultimately death.

A traditional approach to modelling hydrocephalus is a lumped-parameter model where the contents of the skull are represented by a series of interconnected compartments through which fluid is exchanged. All of the resistance to flow between these compartments is lumped at their interfaces. The formulation of such models leads to a system of coupled differential equations for the evolution in time of the fluid pressure in each compartment. The solution of that system gives a relationship between the intracranial pressure and the volume of the ventricles, see for instance Sivaloganathan, Drake & Tenti (1998). Such a pressure–volume relationship is useful in the diagnosis and treatment of hydrocephalus, but as no spatial variation is permitted in any of the physical parameters, it is not possible to describe the stress and strain distributions in the brain tissue or to make predictions regarding the distribution of fluid in hydrocephalus. Such limitations mean that over the last decade, attention has shifted away from lumped-parameter models to the formulation of spatially more realistic models for the hydrocephalic brain.

A number of authors have proposed mechanical models of hydrocephalus based on the theory of poroelasticity. It is hoped that such models will give a better understanding of the condition and hence better treatment. These existing poroelastic models consider hydrocephalus in the final diseased state and do not consider the transition from the healthy to the pathological condition of the brain when there might still be flow through the aqueduct. Nor have such models included the transient effects associated with shunting, the most widely used treatment for hydrocephalus. In this paper, we construct a model of the brain and ventricular system that is sufficiently

https://doi.org/10.1017/S0022112005005707 Published online by Cambridge University Press

complex to reproduce the behaviour of the hydrocephalic brain yet simple enough to be mathematically tractable, and use the model to analyse the onset and treatment of the condition. A review of the general area of application of poroelasticity to the brain may be found in Tenti, Drake & Sivaloganathan (2000).

The use of a mechanical model with a more realistic spherical geometry was first proposed in Hakim, Vanegas & Burton (1976), as was the concept of the brain as a spongelike material. The governing equations formulated by Hakim *et al.* do not, however, incorporate this spongelike behaviour and so are unable to simulate the build-up of fluid in brain tissue (oedema) observed in cases of hydrocephalus.

A crucial step forward was made by Nagashima *et al.* (1987), who used the consolidation theory developed by Biot (1941) to model the brain as a porous linearly elastic solid. This enabled them to formulate governing equations that modelled both the stress and strain distribution and the pressure of distribution of fluid (CSF) through the brain. These authors used a finite-element method to solve their model numerically for an anatomically realistic geometry. While this approach yielded results that were in qualitative agreement with clinical observations, the quantitative accuracy of their results was limited by their use of inaccurate values of some the material parameters and by the boundary conditions used in solving the governing equations.

Kaczmarek, Subramaniam & Neff (1997), Tenti, Sivaloganathan & Drake (1998), Levine (1999) and Taylor & Miller (2004) have attempted to resolve these difficulties with varying degrees of success. In Kaczmarek *et al.* (1997) and Tenti *et al.* (1998), a cylindrical geometry is used in order to facilitate the analytic solution of the governing equations. Such analytic solutions are desirable as they give a deeper insight into the behaviour of pressure and stress through the brain, but the use of such a geometry introduces difficulties, especially when it comes to specifying boundary conditions at the ends of the cylindrical 'brain'. Levine uses a spherically symmetric geometry similar to that in Hakim *et al.* (1976) to construct analytic solutions and Stastna *et al.* (1998) extended the model in Tenti *et al.* (1998) to include some transient effects. Taylor & Miller (2004) use a finite-element method to analyse deformation of a two-dimensional but realistically shaped ventricle.

All of the authors model the brain as a poroelastic solid undergoing small strains. Kaczmarek *et al.* and Tenti *et al.* (1998) use data from a range of medical and anatomical studies to find the values of, for example, the Young's modulus and permeability of the brain tissue. Levine modified previous poroelastic models by attempting to incorporate the absorbtion of fluid in the brain tissue and the effect of the venous bed in the skull. This approach necessitated the use of more physical parameters and the results of Levine and Tenti *et al.* (1998) are qualitative in nature. The model of Kaczmarek *et al.* (1997) provided predictions for flow and stress in the brain tissue. The use of linear elasticity has been considered in a number of papers. Kyriacou *et al.* (2002) compare a linearly elastic model of the form used here with a nonlinear viscoelastic (but not porous) model of Miller & Chinzei (1997). They concluded that for modelling high-strain-rate surgical procedures, the viscoelastic model is most suitable, but that a poroelastic model may be more appropriate for low-strain-rate problems such as hydrocephalus. Taylor & Miller (2004) show that for strains typical in hydrocephalus, the difference in stress predicted by linear and nonlinear elastic models is negligible, so in this paper we use linear elasticity within the poroelastic framework. It is, of course, the case that nonlinear elasticity is necessary for larger strains in models of tissue elsewhere in the body.

In the next section, we set out the results from poroelasticity and fluid flow that we use in our model. Then we describe the assumptions regarding geometry, material

https://doi.org/10.1017/S0022112005005707 Published online by Cambridge University Press

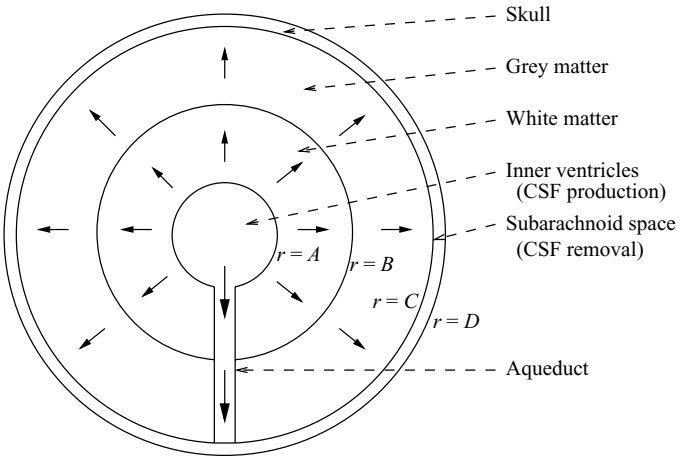


FIGURE 1. Schematic model of the brain, showing inner ventricles, aqueduct, grey and white matter, subarachnoid space (assumed to have negligible thickness) and skull.

properties and time dependence that we make in order to complete a model of hydrocephalus. We then present solutions to the model and consider the physical parameters that we require in order to make quantitative predictions about the behaviour of the brain and CSF. These solutions are discussed in terms of their usefulness relative to some of the other models available and their consistency with clinical data.

2. Mathematical model

In this section, we set out some basic results from poroelasticity and fluid mechanics that underly our model of the brain. As already indicated, the model can be applied to a healthy or a damaged cerebrospinal fluid flow. We will assume that CSF is produced at a constant rate and once produced can (*a*) remain in the ventricle, causing the ventricle to enlarge, (*b*) flow through the aqueduct or (*c*) flow through the porous matrix of brain tissue.

2.1. *Geometry*

We use a spherical geometry based on the first mechanical model for a realistic brain geometry proposed in Hakim *et al.* (1976), see figure 1. The brain is modelled as being composed of two concentric porous linearly elastic thick shells with outer radii B and C, that represent the white and grey matter, respectively. Each layer may have different mechanical properties, reflecting the different properties of each type of tissue. The ventricles are modelled as a single spherical cavity of radius A, located at the centre of the brain, while the dura mater, skull and scalp are represented by a single spherical layer of impermeable solid, outer radius D, enclosing the system. The vessels that connect the ventricles, including the aqueduct of Sylvius, are modelled as a single cylindrical channel and generically denoted the aqueduct. This narrow channel of diameter d runs from the central cavity to the interface between the grey matter and the skull (the subarachnoid space). We suppose that since the volume of this channel is very small relative to the volume of the brain it will have no effect on the solid mechanical properties of the surrounding tissue. The subarachnoid space is treated as a thin layer of negligible thickness where fluid absorption occurs.

https://doi.org/10.1017/S0022112005005707 Published online by Cambridge University Press

Numerical experiments (see below) with the subarachnoid space being treated as a 2 mm thick layer filled with incompressible fluid, show no effect on calculations of pressure or displacement in the brain.

The central cavity is filled with fluid (CSF) of viscosity μ which is produced at a constant rate Q_p. This fluid can flow from the ventricles through both the aqueduct and the porous tissue of the parenchyma into the subarachnoid space, where it is absorbed into the blood. This absorption is assumed to be proportional to the pressure difference between the blood and the CSF in the subarachnoid space. We expect that in the normal physiological state, by far the greatest proportion of fluid movement will occur through the aqueduct. Should this flow be constrained as a result of stenosis of the aqueduct (so that the effective diameter of the aqueduct becomes small) we expect a much greater degree of flow through the brain itself, as happens in patients with hydrocephalus. In the case where a shunt is used to divert CSF into the bloodstream we suppose that fluid is removed directly from the ventricles at a rate Q_S.

The schematic geometry of our model is illustrated in figure 1, and while this represents a significant simplification of the make-up of a real brain we believe that it captures the key geometric and mechanical properties necessary for our purposes. In particular, there is some justification for the use of a spherical model of the ventricles (which in a healthy brain are, in fact, narrow 'C-shaped' cavities) by their approximately spherical configuration which is observed in hydrocephalus.

2.2. *Poroelastic equations*

An isotropic elastic solid subject to a stress field σ_{ij} such that it undergoes a small strain deformation with displacements u_i in the coordinate directions with a resultant strain tensor ϵ_{ij} satisfies the constitutive relationship from Hooke's Law,

$$\epsilon_{ij} = \frac{1}{E}[(1+\nu)\sigma_{ij} - \nu\sigma_{kk}\delta_{ij}], \tag{2.1}$$

where δ_{ij} is the Kronecker delta. The elastic constants E and ν represent the Young's modulus and Poisson's ratio of the material, respectively. The volumetric strain, or dilation, is defined by

$$\varepsilon = \epsilon_{kk} = \frac{\partial u_k}{\partial x_k}. \tag{2.2}$$

The poroelasticity model introduced by Biot (1941) generalized the above equations to model a solid–fluid mixture by introducing a new variable, the fluid pressure, p. Equation (2.1) became

$$\epsilon_{ij} = \frac{1}{E}[(1+\nu)\sigma_{ij} - \nu\sigma_{kk}\delta_{ij}] + \frac{p}{3H}\delta_{ij}, \tag{2.3}$$

where H was a new physical parameter which was regarded as a measure of the mixture's compressibility for a change in fluid pressure.

In order to describe the condition of the body completely we require an additional parameter ζ, the increment of fluid content. A positive value for ζ indicates that fluid has been added by the application of the stress field, a negative value indicates that fluid has been removed. By considering the isotropy of the body and assuming the existence of a potential energy of the mixture it can be shown (see, for example, Wang 2002) that ζ is given by

$$\zeta = \frac{1}{H}\sigma_{kk} + \frac{p}{G}. \tag{2.4}$$

https://doi.org/10.1017/S0022112005005707 Published online by Cambridge University Press

G is another new physical constant that describes the change in fluid content for a given change in fluid pressure.

We now invert (2.3) to give

$$\sigma_{ij} = \frac{E}{1+\nu}\epsilon_{ij} + \frac{\nu E}{(1+\nu)(1-2\nu)}\varepsilon\delta_{ij} - \alpha p\delta_{ij}, \tag{2.5}$$

where the Biot–Willis parameter α is another poroelastic constant defined as

$$\alpha = \tfrac{1}{3}\frac{E}{(1-2\nu)H}.$$

The expression for the increment of fluid content (2.4) can be rewritten in terms of the strain

$$\zeta = \alpha\varepsilon + \frac{(1-\alpha\beta)\alpha}{K\beta}p. \tag{2.6}$$

In this expression, K is the bulk modulus of the body,

$$K = \frac{E}{3(1-2\nu)},$$

and we denote Skempton's coefficient as β,

$$\beta = \frac{G}{H},$$

where β is essentially a measure of how the applied stress is distributed between the solid matrix and the fluid. It tends to unity for saturated mixtures where the load is supported entirely by the fluid and zero for gas-filled pores where the stress is transferred through the solid. By setting $p=0$ in (2.6), we can see that α may be interpreted as the ratio of volume of fluid displaced to the volumetric strain under drained conditions.

Note that in poroelasticity theory there exists a range of different material constants (such as G, H, α and β) that characterize the behaviour of the fluid–solid mixture, see Wang (2002) for an exhaustive list. There are, however, only two distinct constants which, together with two elastic constants representing the average elastic properties of the solid matrix, fully describe the material properties of the body. This is analogous to the case of isotropic linear elasticity where only two constants are ever required to completely specify the elastic properties of a material, but several elastic moduli are defined and used in practice. For consistency and simplicity we shall use E, ν, α and β as the four independent material constants. We do, however, observe that two more constants, the undrained Poisson's ratio ν_{u} and the undrained Young's modulus E_{u}, can be defined as

$$\nu_{\mathrm{u}} = \frac{3\nu + \alpha\beta(1-2\nu)}{3-\alpha\beta(1-2\nu)}, \quad E_{\mathrm{u}} = \frac{(1-2\nu_{\mathrm{u}})}{(1-2\nu)}\frac{E}{1-\alpha\beta}. \tag{2.7a, b}$$

Our reason for making these additional definitions will become evident when we consider the values of the material parameters to be used in our model.

We also observe that the total stress tensor of the mixture, σ_{ij}, may be regarded as an additive mixture of the fluid pressure p and the 'effective stress' in the solid matrix σ'_{ij},

$$\sigma_{ij} = \sigma'_{ij} - \alpha p\delta_{ij}. \tag{2.8}$$

The negative sign on the pressure follows from the convention in solid mechanics that pressures are positive and compressive stresses negative. This idea of the separation

https://doi.org/10.1017/S0022112005005707 Published online by Cambridge University Press

of the total stress into solid and fluid components will be useful in the application of the boundary conditions.

2.3. *Fluid flow equations*

In order to complete a model for the behaviour of the fluid–solid mixture we also require an expression for the movement of fluid through the solid matrix and the aqueduct.

We assume Darcy flow for movement of fluid through the porous brain parenchyma, which for spherically symmetric flow at radius r, is

$$W = -\frac{k}{\mu}\frac{\partial p}{\partial r}, \tag{2.9}$$

where W denotes the flow relative to the solid per unit area, or filtration velocity, μ is the viscosity of the fluid and k is the permeability of the matrix, which will, in general, be strain dependent. Klachnar & Tarbell (1987) proposed modelling the permeability of arterial tissue as an exponentially increasing function of the strain. Kaczmarek *et al.* (1997) suggested a small-strain linear approximation between the inverse permeability and the strain. A model of either form introduces a material parameter that has unknown value, so in this work we keep the permeability constant and accept that one of the important elements of poroelasticity, linkage between the permeability and strain, must await better measurements of the physical properties of the parenchyma.

For flow through the vessels connecting the ventricles (our aqueduct) we assume Poiseuille flow through a straight cylindrical tube, so that

$$Q_a = \frac{\pi d^4}{128\mu L}(p_A - p_C), \tag{2.10}$$

where Q_a is the volume of fluid flowing per unit time, d is the diameter of the tube, L is the length of the tube and p_A and p_C are the pressures at either end.

2.4. *Material properties*

Perhaps the most important decision to be made in modelling the material properties of the brain tissue involves the choice of constitutive equation for the solid matrix. It is well known that biological soft tissues rarely obey Hooke's law, but instead exhibit a mechanically nonlinear stress–strain relationship (see Sahay 1984; Fung 1993). Some progress has been made in the formulation of such a nonlinear model for the brain, based on the theory of hyperelasticity (see Sahay *et al.* 1992; Miller & Chinzei 1997). Sahay & Kothiyal (1984) even modelled the intracranial pressure–volume relationship in this fashion. They were, however, unable to reproduce the behaviour of the brain under pressure, most probably because their model was unable to incorporate the porous nature of the parenchyma. Indeed, it seems that at present no theoretical basis for modelling a mechanically nonlinear poroelastic material exists. We therefore follow all of the previous authors in the field (see for instance Miller 1999; Kyriacou *et al.* 2002; Taylor & Miller 2004) by using a Hookean form for the stress–strain behaviour of the brain. Since the white and grey matter may, in general, be expected to exhibit different material properties, we denote the Poisson's ratios and Young's moduli of each as ν_w and ν_g and E_w and E_g. As indicated above, the white and grey matter are taken to have constant permeability, k_w and k_g, respectively. The most recent experimental evidence suggests that the poroelastic properties of the white and grey matter should be taken to be the same, but we retain the ability to distinguish the two regions of parenchyma.

https://doi.org/10.1017/S0022112005005707 Published online by Cambridge University Press

The outer layer consisting of the dura mater, skull and scalp is taken to be homogenous with elasticity constants ν_s and E_s and zero permeability. While in reality each of the three components of this layer will exhibit distinct material properties, we justify our assumption of homogeneity by suggesting that only the comparatively very rigid skull is likely to be of mechanical significance. Since the grey matter and the outer layer of tissue are in contact in our model, we suppose that the radial displacement and stress will be continuous at the interface ($r = C$). At the interface between the white and grey matter ($r = B$), we must impose the condition that the displacement, radial stress, fluid pressure and flow rate are all continuous.

2.5. *Quasi-steady approximation*

In formulating the governing equations for our model, we shall consider only the quasi-steady behaviour of the system as the evolution of hydrocephalus occurs on a time scale of days and weeks (Hakim *et al.* 1976), inertial terms in the governing equations which represent the propagation of waves through the tissue are unlikely to affect the process of the brain settling into a hydrocephalic state. This conclusion is supported by the work of Stastna *et al.* (1998) who showed that the retention of such terms led to waves propagating on a time scale of order 10^{-2} s, much too short a time to affect the onset of the condition.

Thus by assuming changes happen slowly, we introduce time dependence to the behaviour of the ventricle walls, the displacement of which will be of critical importance in the comparison of our results with clinical observations. We model the time rate of change of the volume of the ventricular cavity as being equal to the difference between the production rate of CSF and the total drainage rate through the aqueduct, parenchyma and any shunting device present, see (4.1). This will allow us to construct a phase plot of the behaviour of the ventricle wall, and hence to investigate the stability or otherwise of our steady-state solutions. We will also be able to analyse how some variation in the material parameters affects the position and stability of the steady state.

2.6. *Onset and treatments*

The model allows investigation of the onset of hydrocephalus in a number of ways. Stenosis of the aqueduct, the main cause of the illness, can be modelled by reducing the value of the aqueduct diameter, d. We further simulate hydrocephalus from impaired absorption in the subarachnoid space. We are able also to consider the effect of treatments, in particular shunting, on the subsequent mechanical behaviour of the brain.

Using a phenomenological model for the quantitative properties of shunts based on the results recorded by Czosnyka *et al.* (1997), we suppose that the flow rate through the shunt, Q_S, driven by a pressure difference between the ventricle and the blood, $\Delta p = p_w(A, t) - p_{bp}$, takes the form

$$Q_S = \begin{cases} S_1 \Delta p & \text{for} \quad \Delta p > 0, \\ 0 & \text{for} \quad \Delta p \leqslant 0, \end{cases} \tag{2.11}$$

for 'ball on spring' devices and

$$Q_S = \begin{cases} S_2 \Delta p + S_3 \Delta p^2 & \text{for} \quad \Delta p > 0, \\ 0 & \text{for} \quad \Delta p \leqslant 0, \end{cases} \tag{2.12}$$

for shunts with silicone diaphragm valves. Here, S_1–S_3 are physical parameters that will depend on the material properties of the shunt, $p_w(A, t)$ is the CSF pressure in the ventricles and p_{bp} is the blood pressure.

https://doi.org/10.1017/S0022112005005707 Published online by Cambridge University Press

Other methods of treating hydrocephalus can also be studied using the model. A surgical procedure to widen the aqueduct (the removal of a tumour, say) could be represented by increasing d after it had been constricted for some time. We can use the quasi-steady model to study the effect of a lumbar puncture by instantaneously reducing the volume of the ventricles and observing how, or indeed if, they return to a deformed configuration.

3. Hydroelastic system of equations

3.1. *Fluid*

The continuity equation for spherical flow with velocity V of an incompressible fluid in a biphasic medium is

$$\frac{\partial \zeta}{\partial t} + \frac{1}{r^2}\frac{\partial}{\partial r} r^2 V + Q_{\mathrm{ab}} = 0, \tag{3.1}$$

where flux can be decomposed in terms of the fluid velocity W and the matrix velocity u_t as

$$V = W + u_t.$$

Applying our assumptions of quasi-steady state and no CSF absorption in the brain, we find that the equilibrium equation for the fluid is simply

$$\frac{\partial W}{\partial r} + \frac{2W}{r} = 0.$$

Now we apply Darcy's Law, (2.9), to express the filtration velocity in terms of the pressure and then split the domain into the white matter $A \leqslant r < B$ and grey matter $B \leqslant r < C$, so that the governing equations for the fluid pressure in the white matter, p_w, and grey matter, p_g, are

$$\frac{\partial^2 p_w}{\partial r^2} + \frac{2}{r}\frac{\partial p_w}{\partial r} = 0 \quad (A \leqslant r \leqslant B), \tag{3.2}$$

and

$$\frac{\partial^2 p_g}{\partial r^2} + \frac{2}{r}\frac{\partial p_g}{\partial r} = 0 \quad (B \leqslant r \leqslant C). \tag{3.3}$$

We do not include expressions for the pressure in the region $C \leqslant r \leqslant D$ since no fluid is present in that part of the domain.

3.2. *Solid matrix equations*

The governing equations for the solid phase are derived from the poroelastic equations for spherically symmetric deformation, again assuming quasi-steady conditions.

The strains and the dilation are given in terms of the radial displacement, u, by

$$\epsilon_{rr} = \frac{\partial u}{\partial r}, \quad \epsilon_{\theta\theta} = \epsilon_{\phi\phi} = \frac{u}{r}, \quad \epsilon_{r\theta} = \epsilon_{\theta\phi} = \epsilon_{\phi r} = 0,$$

$$\varepsilon = \epsilon_{rr} + \epsilon_{\theta\theta} + \epsilon_{\phi\phi} = \frac{\partial u}{\partial r} + 2\frac{u}{r}.$$

https://doi.org/10.1017/S0022112005005707 Published online by Cambridge University Press

Substituting these expressions into (2.5) leads to expressions for the stresses,

$$\left.\begin{aligned}
\sigma_{rr} &= \frac{E(1-\nu)}{(1+\nu)(1-2\nu)}\frac{\partial u}{\partial r} + \frac{2E\nu}{(1+\nu)(1-2\nu)}\frac{u}{r} - \alpha p,\\
\sigma_{\theta\theta} = \sigma_{\phi\phi} &= \frac{E\nu}{(1+\nu)(1-2\nu)}\frac{\partial u}{\partial r} + \frac{E}{(1+\nu)(1-2\nu)}\frac{u}{r} - \alpha p,\\
\sigma_{r\theta} = \sigma_{\theta\phi} &= \sigma_{\phi r} = 0.
\end{aligned}\right\} \tag{3.4}$$

Since there are no body forces and using the quasi-steady approximation, the stress is divergence free, giving

$$\frac{\partial \sigma_{rr}}{\partial r} + \frac{1}{r}(2\sigma_{rr} - \sigma_{\theta\theta} - \sigma_{\phi\phi}) = 0.$$

We now substitute (3.4) into the above equation to find the governing equations for the displacement of the white matter u_w,

$$\frac{\partial^2 u_w}{\partial r^2} + \frac{2}{r}\frac{\partial u_w}{\partial r} - 2\frac{u_w}{r^2} = E_w^*\frac{\partial p_w}{\partial r} \quad (A \leqslant r \leqslant B), \tag{3.5}$$

and of the grey matter u_g,

$$\frac{\partial^2 u_g}{\partial r^2} + \frac{2}{r}\frac{\partial u_g}{\partial r} - 2\frac{u_g}{r^2} = E_g^*\frac{\partial p_g}{\partial r} \quad (B \leqslant r \leqslant C), \tag{3.6}$$

where

$$E_w^* = \alpha\frac{(1+\nu_w)(1-2\nu_w)}{E_w(1-\nu_w)}, \quad E_g^* = \alpha\frac{(1+\nu_g)(1-2\nu_g)}{E_g(1-\nu_g)}.$$

We can simply perform the above analysis with $p = 0$ to find the governing equation for the displacement of the impermeable outer layer of tissue (the skull), u_s,

$$\frac{\partial^2 u_s}{\partial r^2} + \frac{2}{r}\frac{\partial u_s}{\partial r} - 2\frac{u_s}{r^2} = 0 \quad (C \leqslant r \leqslant D). \tag{3.7}$$

We now have a set of governing equations (3.2)–(3.3) and (3.5)–(3.7) that describe the behaviour of the independent variables for pressure and displacement.

4. Boundary conditions

The model system has five second-order equations. We therefore require ten boundary conditions in order to completely solve the system; four on the pressure/fluid velocity and six on the displacement/solid stress. We apply two boundary conditions at the ventricle wall ($r = A$), four at the interface between the white and grey matter ($r = B$), three at the interface of the grey matter and the skull ($r = C$) and one at the outer surface of the skull ($r = D$).

4.1. *Ventricles*

The boundary condition for the pressure in the ventricles, $p_w(A, t)$, is the most complicated and perhaps the most important that we shall apply. It is here where we incorporate the flow of fluid through the aqueduct and shunting into the model. The deformation of the ventricles is also the clearest clinical sign of hydrocephalus, so the size of the radial deformation of the ventricle wall, $u_w(A, t)$, will be important in evaluating the model.

https://doi.org/10.1017/S0022112005005707 Published online by Cambridge University Press

Using a quasi-steady approximation and allowing the ventricle radius to vary slowly, we introduce a term $\dot{V}$, the rate of change of the ventricular volume with respect to time so that conservation of CSF gives:

$$\dot{V} = \overbrace{Q_p}^{\text{I}} - \overbrace{\frac{\pi d^4}{128\mu L}[p_w(A) - p_g(C)]}^{\text{II}} + \overbrace{4\pi A^2 \frac{k_w}{\mu}\frac{\partial p_w}{\partial r}\bigg|_{r=A}}^{\text{III}} - \overbrace{S(p_w(A))}^{\text{IV}}. \tag{4.1}$$

The first term gives the constant production of CSF. The second term gives the flow of fluid through the aqueduct, Q_a, driven by the pressure difference between the ventricles and the subarachnoid space $[p_w(A) - p_g(C)]$. The parameters d and L represent an effective diameter and length of the aqueduct, respectively, see (2.10). If the aqueduct is being forced into collapse then it will not remain cylindrical; however, its length will not change much so we continue to use a Poiseuille-flow approximation, but interpret d as the diameter of a cylindrical tube with the same flow rate for a given pressure drop. The third term models the flow of fluid across the ventricle wall into the parenchyma using the velocity of the flow from Darcy's law (2.9). The fourth term is the flow rate through any shunt. If steady state has been reached, then $\dot{V} = 0$. Now expressing the ventricular volume in terms of the initial radius A and the deformation of the ventricle, $u_w(A, t)$,

$$\dot{V} = \frac{\mathrm{d}}{\mathrm{d}t}\left[\tfrac{4}{3}\pi(A + u_w(A, t))^3\right].$$

Substituting into (4.1) we have a first-order nonlinear differential equation for $u_w(A, t) \equiv u_A(t)$,

$$\frac{\mathrm{d}u_A}{\mathrm{d}t} = \frac{1}{4\pi(u_A(t) + A)^2}\left[Q_p - \frac{\pi d^4}{128\mu L}[p_w(A, t) - p_g(C, t)] + 4\pi A^2 \frac{k_w}{\mu}\frac{\partial p_w}{\partial r}\bigg|_{r=A} - S(p_w(A, t))\right]. \tag{4.2}$$

The second boundary condition to be applied here refers to the solid matrix. Since the brain is untethered at the ventricle wall we assume that the stress, σ_{rr}, balances against the fluid pressure in the ventricle, so that the solid stress, σ'_{rr}, satisfies at $r = A$,

$$\sigma'_{rr} = \sigma_{rr} + \alpha p = (\alpha - 1)p,$$

and thus σ'_{rr} will be zero when $\alpha = 1$. Hence, the second boundary condition is

$$\frac{E_w(1 - \nu_w)}{(1 + \nu_w)(1 - 2\nu_w)}\frac{\partial u_w}{\partial r}\bigg|_{r=A} + \frac{2E_w\nu_w}{(1 + \nu_w)(1 - 2\nu_w)}\frac{u_w(A, t)}{A} = (\alpha - 1)p_w(A). \tag{4.3}$$

4.2. *Interface of white and grey matter*

The four boundary conditions to be applied at $r = B$ all come from the continuity of physical quantities in our model; the displacement, radial stress, fluid pressure and filtration velocity must all be continuous. Hence, we match displacements

$$u_w(B, t) = u_g(B, t), \tag{4.4}$$

and stresses

https://doi.org/10.1017/S0022112005005707 Published online by Cambridge University Press

$$\frac{E_w(1-\nu_w)}{(1+\nu_w)(1-2\nu_w)}\frac{\partial u_w}{\partial r}\bigg|_{r=B}+\frac{2E_w\nu_w}{(1+\nu_w)(1-2\nu_w)}\frac{u_w(B,t)}{B}-\alpha p_w(B,t)$$
$$=\frac{E_g(1-\nu_g)}{(1+\nu_g)(1-2\nu_g)}\frac{\partial u_g}{\partial r}\bigg|_{r=B}+\frac{2E_g\nu_g}{(1+\nu_g)(1-2\nu_g)}\frac{u_g(B,t)}{B}-\alpha p_g(B,t). \quad (4.5)$$

in the solid. Note that since the αp terms will cancel from each side of the equation, it does not matter whether we choose to equate the effective stresses $\sigma'_{rr}(B)$ or total stresses $\sigma_{rr}(B)$.

We also match fluid pressures

$$p_w(B,t)=p_g(B,t) \quad (4.6)$$

and filtration velocities

$$-\frac{k_w}{\mu}\frac{\partial p_w}{\partial r}\bigg|_{r=B}=-\frac{k_g}{\mu}\frac{\partial p_g}{\partial r}\bigg|_{r=B} \quad (4.7)$$

across the interface.

4.3. *Subarachnoid space*

The first two boundary conditions at $r=C$ are a result of the continuity of the behaviour of the solid between the brain and the skull. Thus, we apply continuity of displacements

$$u_g(C,t)=u_s(C,t), \quad (4.8)$$

and stresses

$$E_g\left(\frac{1-\nu_g}{(1+\nu_g)(1-2\nu_g)}\right)\frac{\mathrm{d}u_g}{\mathrm{d}r}\bigg|_{r=C}+\frac{2E_g\nu_g}{(1+\nu_g)(1-2\nu_g)}\frac{u_g(C)}{C}-\alpha p_w(C,t)$$
$$=E_s\left(\frac{1-\nu_s}{(1+\nu_s)(1-2\nu_s)}\right)\frac{\mathrm{d}u_s}{\mathrm{d}r}\bigg|_{r=C}+\frac{2E_s\nu_s}{(1+\nu_s)(1-2\nu_s)}\frac{u_s(C,t)}{C}, \quad (4.9)$$

in a similar way to those at the interface of the white and grey matter.

The third boundary condition relates to the absorption of fluid which occurs in the subarachnoid space. Modelling the absorption as proportional to the pressure difference between the CSF and the bloodstream, we find that

$$\frac{p_g(C,t)-p_{bp}}{R\mu}=\frac{\pi d^4}{128\mu L}[p_w(A,t)-p_g(C,t)]-4\pi C^2\frac{k_g}{\mu}\frac{\partial p_g}{\partial r}\bigg|_{r=C}. \quad (4.10)$$

The term on the left-hand side of this equation refers to the flow of fluid through the arachnoid villi, which is driven by the pressure difference $(p_g(C)-p_{bp})$ and where R is a parameter that models the resistivity of the villi to flow. Note that since flow cannot occur from the blood into the subarachnoid space, we implicitly assume that in all cases $p_g(C)\geqslant p_{bp}$.

4.4. *Skull*

The last boundary condition applies to the outside of the skull, $r=D$. Here, we simply assume that the solid is untethered and hence stress free so that

$$E_s\left(\frac{1-\nu_s}{(1+\nu_s)(1-2\nu_s)}\right)\frac{\mathrm{d}u_s}{\mathrm{d}r}\bigg|_{r=D}+\frac{2E_s\nu_s}{(1+\nu_s)(1-2\nu_s)}\frac{u_s(D,t)}{D}=0. \quad (4.11)$$

The total stress and effective stress are identical here since there is no fluid pressure, hence there is no need to make any distinction between them in applying this boundary condition.

https://doi.org/10.1017/S0022112005005707 Published online by Cambridge University Press

4.5. *Solution method*

The formulation we have derived provides us with a set of ten boundary conditions, (4.1) and (4.3)–(4.11) with which to solve the governing equations (3.2)–(3.3) and (3.5)–(3.7). The spherical geometry allows the pressure and displacement to be determined in terms of simple powers of the radial distance and unknown constants. In the steady case, the solutions, when substituted into the boundary conditions, thus reduce to solving a 10×10 linear system for the unknown constants. This has been done using *Maple* to solve the linear system analytically. In the unsteady case, the nine boundary conditions (4.3)–(4.11) are applied, leaving just the ventricle displacement undetermined. Equation (4.2) can then be solved numerically using *MATLAB* to provide the time evolution of the deformation of the ventricle wall and corresponding stress and displacement within the grey and white matter, for full details see Smillie (2003). In addition to following the time evolution, we also use a phase plot of u_A *vs.* $\mathrm{d}u_A/\mathrm{d}t$ to determine the stability of a steady-state solution to the model.

5. Parameter estimation

The evaluation of the material parameters is often a non-trivial problem in biomechanics since the usual engineering tests used to measure the physical properties of a material are often difficult to apply to soft biological tissue. There is also the question of different material behaviour *in vivo* and *in vitro*, with experimentation in the former case being ethically, as well as practically, problematic. In the following section, we shall therefore attempt to estimate numerical values for all of the parameters in our model, but some will inevitably be rough approximations.

5.1. *Geometry of the brain*

Since the spherically symmetric geometry of the brain in the model is an idealization we must calculate values for A, B, C, D, L and d that are in some sense equivalent to those in the real geometry. We use values for the radii of the ventricles, white matter and grey matter that approximately correspond to their location in the adult male brain as in Kaczmarek *et al.* (1997). Hence, we find that the ventricles are of radius $A = 30\,\mathrm{mm}$, the interface of the white and grey matter is at $B = 70\,\mathrm{mm}$ and the brain itself has radius $C = 100\,\mathrm{mm}$. Taking the skull to be of thickness 2 mm (Drossos, Santomaa & Kuster 2000), the outer layer of the model will be of radius $D = 102\,\mathrm{mm}$.

The diameter of a healthy cerebral aqueduct varies along its length and between individuals; we use the average value reported in Bickers & Adams (1949), $d = 4\,\mathrm{mm}$. Since we have assumed that the aqueduct is straight and runs from the ventricles to the subarachnoid space, we suppose that it is of length $L = C - A = 70\,\mathrm{mm}$.

5.2. *Poroelastic constants*

The poroelastic constants are perhaps the most difficult set of parameters for which to find numerical values. Kaczmarek *et al.* (1997) use a value of $E = 10\,\mathrm{kPa}$ for the Young's modulus, taken from Metz, McElhaney & Ommaya (1970). As was noted in Levine (1999), however, this represents the instantaneous, or undrained, value of the coefficient, the drained value is likely to be somewhat smaller. It is also unclear whether the value of the Poisson's ratio used, $\nu = 0.35$, was measured under drained or undrained conditions.

In formulating a model of the brain, all previous authors have assumed that the brain is perfectly saturated so that $\alpha = \beta = 1$. In order to enable us to convert from undrained to drained elastic moduli, we instead suppose that the brain is almost, but

https://doi.org/10.1017/S0022112005005707 Published online by Cambridge University Press

not perfectly, saturated with fluid, and use the values given in Wang (2002) for such a mixture,

$$\alpha = 1, \quad \beta = 0.99.$$

Now, if the value of ν quoted above refers to drained conditions then, using (2.7), we find that the undrained Poisson's ratio is

$$\nu_u = 0.4983,$$

that is, the mixture is virtually incompressible under undrained conditions. This may explain why Nagashima *et al.* erroneously used a value of $\nu = 0.4999$ in their model of the hydrocephalic brain. Given an undrained Young's modulus of $E_u = 10\,\mathrm{kPa}$ and inverting (2.7*b*), the value of the drained Young's modulus is

$$E = \frac{1-2\nu}{1-2\nu_u} E_u(1-\alpha\beta) = 9010\,\mathrm{Pa},$$

only a little lower than the value used by Kaczmarek *et al.*

However, if the value of the Poisson's ratio used in Kaczmarek *et al.* (1997) was measured under undrained conditions (so that $\nu_u = 0.35$), we find that the drained value of the Poisson's ratio is

$$\nu = \frac{3\nu_u - \alpha\beta(1+\nu_u)}{3-2\alpha\beta(1+\nu_u)} = -0.876,$$

a value of ν that is unusual, but not physically inadmissible. Materials with negative Poisson's ratio exist and are thought to occur in other places in the body, see for example Lakes (1993, 2002), so while the suggestion of a negative Poisson's ratio for brain tissue is highly unusual, it is not an impossible suggestion. Again assuming that $E_u = 1 \times 10^4\,\mathrm{N\,m^{-2}}$, we then have a Young's modulus of

$$E = 918\,\mathrm{Pa},$$

an order of magnitude lower than that used by Kaczmarek *et al.*

Taylor & Miller (2004) suggest that these values are too high and that the appropriate value of Young's modulus is $E = 584\,\mathrm{Pa}$ and we use that value as a standard in the calculations below.

The estimates of E were measured using a section of brain composed mainly of white matter. In the absence of any quantitative data regarding different elastic properties of the grey matter we will assume as a standard that $E_w = E_g = E$ and $\nu_w = \nu_g = \nu$ when computing results, though in reality it is likely that the grey matter will be a little stiffer.

For the skull we use values of

$$E_s = 1 \times 10^9\,\mathrm{Pa}, \quad \nu_s = 0.3,$$

from van Rietbergen *et al.* (1995).

In order to fully characterize the poroelastic behaviour of the brain we require numerical values for the permeabilities k_w and k_g. Kaczmarek *et al.* calculated the permeability of the white matter using the results of Reulen *et al.* (1977) (note that the value given as 'permeability' in their paper is the permeability scaled by fluid viscosity). Based on their calculations, the appropriate value for the permeability of the white matter is

$$k_w = 1.4 \times 10^{-14}\,\mathrm{m^2}.$$

https://doi.org/10.1017/S0022112005005707 Published online by Cambridge University Press

They considered that the permeability of grey matter should be smaller and used a value

$$k_g = 1.4 \times 10^{-16}\,\mathrm{m}^2,$$

but this value leads to unrealisticly large transparenchymal pressure differences, so as a standard case we follow Taylor & Miller (2004) and set the permeability for both white and grey matter to be the same higher value. We consider below the effect of varying the permeability of the grey matter.

5.3. *Fluid flow and drainage*

The physical properties of the CSF system itself are rather better documented. Since CSF has physical properties similar to water, we assume that it has dynamic viscosity (Fay 1994)

$$\mu = 8.9 \times 10^{-4}\,\mathrm{N\,s\,m}^{-2}.$$

This falls within the range of values for CSF at body temperature given by Bloomfield, Johnston & Bilston (1998): $\mu = 7 - 10 \times 10^{-4}\,\mathrm{N\,s\,m}^{-2}$.

The production rate of CSF in the ventricles is reported to be (Bradbury 1993)

$$Q_p = 5.8 \times 10^{-9}\,\mathrm{m}^3\,\mathrm{s}^{-1},$$

which we take to be independent of intraventricular pressure.

We can compare the relative importance of the aqueduct and the porous brain in draining fluid from the ventricles. Taking a typical length scale of L and pressure scale of P and dividing term II of (4.1) by term III gives

$$\frac{\pi d^4 P/128\mu L}{4\pi A^2 k_w P/\mu L} \approx 1750.$$

Thus, in a healthy brain, flow through the aqueduct accounts for virtually all of the transfer of CSF through the ventricular system. Only in a pathological state, for example when $d \to 0$, will a significant proportion of flow occur through the parenchyma. We therefore find that a typical flow velocity in the aqueduct is

$$U = \frac{4Q_p}{\pi d^2} = 0.12\,\mathrm{mm\,s}^{-1}.$$

Then, given a kinematic viscosity $\mu/\rho = 8.9 \times 10^{-7}\,\mathrm{m}^2\,\mathrm{s}^{-1}$, the Reynolds number for flow in the aqueduct is

$$\mathrm{Re} = \frac{\rho U L}{\mu} \approx 10^{-1}.$$

The resistance of the arachnoid villi is well documented, for instance observations on healthy subjects by Albeck *et al.* (1991). They measured the rate of absorption of fluid as the intracranial pressure was varied and from that determined a range for the conductance ($(R\mu)^{-1}$). Converting this value to our variable R gives a range $7-9 \times 10^{13}\,\mathrm{m}^{-3}$. We suppose that the resistance is such that the rate of outflow is exactly equal to the CSF production rate Q_p for a normal physiological value of $p_g(C) - p_{bp} \sim 440\,\mathrm{Pa}$. Hence,

$$R = \frac{[p_g(C) - p_{bp}]_{norm}}{\mu Q_p} = 8.5 \times 10^{13}\,\mathrm{m}^{-3}.$$

We consider below the effect of variation in the resistance, R.

https://doi.org/10.1017/S0022112005005707 Published online by Cambridge University Press

A	30 mm	E_w	584 Pa
B	70 mm	E_g	584 Pa
C	100 mm	E_s	1×10^9 Pa
D	102 mm	ν	0.35
L	70 mm	ν_s	0.3
d	4 mm	μ	8.9×10^{-4} N s m^{-2}
α, β	1, 0.99	Q_p	5.8×10^{-9} m^3 s^{-1}
k_w	1.4×10^{-14} m^2	R	8.5×10^{13} m^{-3}
k_g	1.4×10^{-14} m^2	p_{bp}	650 Pa

TABLE 1. Values of physical constants used to calculate 'standard' model solutions.

We assume a typical value for venous blood pressure of $p_{bp} = 650$ Pa although calculations show little sensitivity to the value used for p_{bp} and values as high as 1100 Pa could be applied.

In order to determine values for S_1, S_2 and S_3, the parameters governing flow through a shunt, we use a least-squares fit to the data in Czosnyka *et al.* (1997) to give $S_1 = 1.25 \times 10^{-10}$ m^5 N s^{-1}, $S_2 = 3.03 \times 10^{-11}$ m^5 N s^{-1} and $S_3 = 3.77 \times 10^{-14}$ m^7 N^{-2} s^{-1}. A summary of a 'standard' set of parameter values is given in table 1.

6. Results

We now consider solutions of the model to test against clinical observations and to examine the behaviour of the response of the brain to a variation in these parameters. The major indicators we consider are the displacement of the ventricle wall, $u_w(A, t)$, and the transparenchymal pressure, $p_w(A, t) - p_g(C)$, since these are the key clinical signs of hydrocephalus. The ventricular aspect ratio,

$$\Gamma = \frac{C + u_g(C, t)}{A + u_w(A, t)},$$

was introduced by Hakim *et al.* (1976) as an alternative measure of the extent of hydrocephalus, we estimate that when making a comparison with the results of those authors. We shall also use the notion of the magnitude of the shear stress

$$|\tau(r, t)| = \frac{|\sigma_r(r, t) - \sigma_\theta(r, t)|}{2}$$

as a measure of tissue damage (see Holbourn 1943).

6.1. *Severe hydrocephalus*

We begin by solving the model for the case of complete occlusion of the aqueduct, $d = 0$, and no shunt, $Q_S = 0$. In this case it is to be expected that the intraventricular pressure will be significantly above normal physiological values, since all of the CSF produced in the ventricles must be driven through the parenchyma, a much more resistant pathway than the aqueduct. This pressure rise will induce a deformation in the parenchyma, the defining symptom of hydrocephalus.

Setting $d = 0$ is also a useful starting point since the results from this configuration of the model can be compared not only with clinical observations of severe hydrocephalus, but also with the other mathematical models of this condition (for example Kaczmarek *et al.* 1997; Tenti *et al.* 1998).

https://doi.org/10.1017/S0022112005005707 Published online by Cambridge University Press

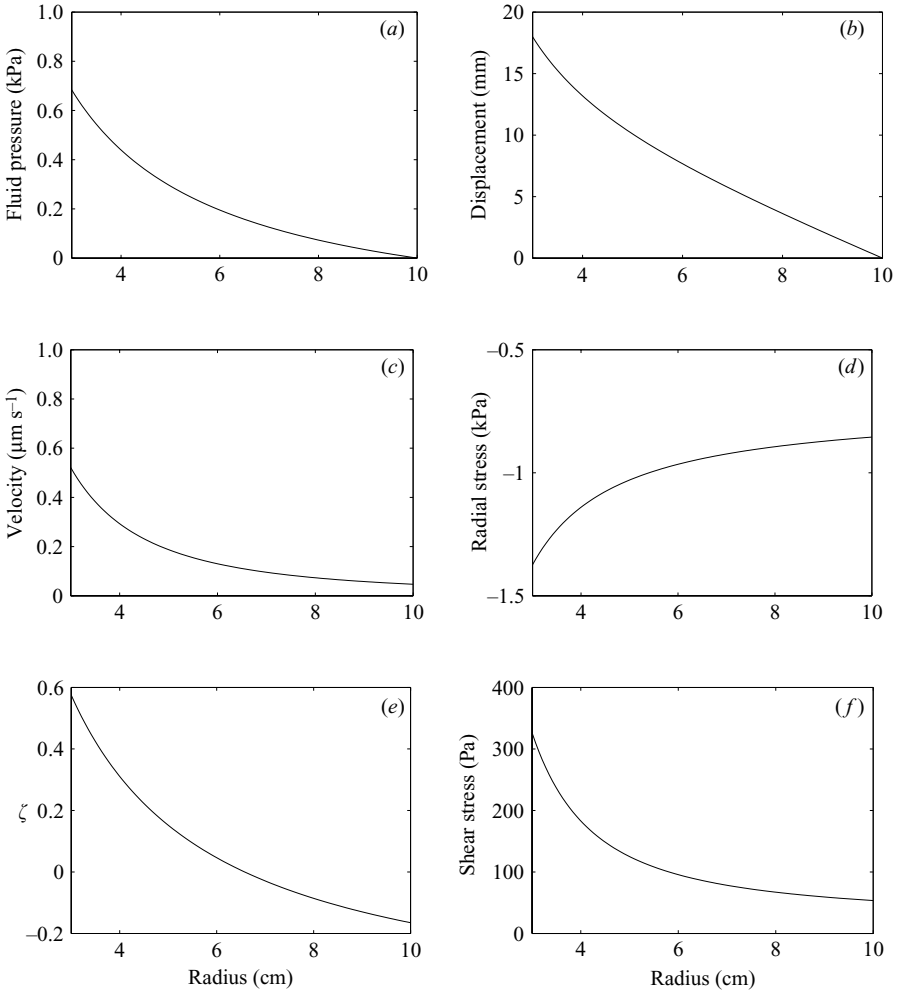


FIGURE 2. Complete occlusion: calculated values in parenchyma of (*a*) fluid pressure relative to subarachnoid pressure, (*b*) displacement, (*c*) superficial fluid velocity, (*d*) radial stress, (*e*) fluid increment, (*f*) shear stress.

6.1.1. *Flow and pressure distribution of CSF*

In figure 2(*a*), we show the excess in pore pressure over pressure in the subarachnoid space. Note that values are plotted against the undeformed radius of the brain. The pressure difference between the ventricle and the subarachnoid space, $p_w(A) - p_g(C)$, is around 660 Pa which seems to be well within the range of physiological values.

The pressure falls off relatively quickly through the white matter, but then decreases more slowly in the grey-matter region of the brain.

In steady state, the volume of fluid flowing out through the arachnoid villi and into the bloodstream is constant, regardless of whether the fluid has arrived in the subarachnoid space via the aqueduct or the parenchyma. This means that in our model, as a consequence of (4.10), the pressure in the subarachnoid space $p_g(C)$ will be always be relatively the same compared to blood pressure and just sufficient to maintain flow through the subarachnoid villi. For the CSF production rate and

https://doi.org/10.1017/S0022112005005707 Published online by Cambridge University Press

resitance, we assume, as noted above, this is a pressure in the subaracnoid space around 440 Pa above venous pressure.

Figure 2(*c*) shows the filtration velocity decreasing as the square of the radius. This is expected since no fluid is absorbed as it passes through the brain, hence the volume of fluid flowing through any given spherical surface should be constant. The filtration velocity is much higher in this case than the typical flow speed estimated in § 5.3. As the volume of CSF has risen, the residence time for the CSF will be greater, but the time spent in the parenchyma will be less, and such a change may have further consequences for the brain if the CSF plays a role in transferring nutrients from the ventricles to the subarchnoid space through the parenchyma.

6.1.2. *Displacements and stresses through the brain*

The radial displacement of the brain is shown in figure 2(*b*). The displacement of the ventricle wall $u_w(A)$, which we shall consider to be the result most indicative of the extent of hydrocephalus, is around 18 mm, while the outer surface of the brain experiences virtually no deformation, a consequence of the relatively rigid nature of the skull. This gives a ventricular aspect ratio of

$$\frac{C + u_g(C)}{A + u_w(A)} = 2.1,$$

which is very close to the value of 2 given in Hakim *et al.* (1976) for a typical case of adult hydrocephalus. The results for the displacement are similar to those in Kaczmarek *et al.* (1997).

The radial stress distributions are shown in figure 2(*d*). The negativity of the total stresses indicates that the stresses are compressive in nature. The stress falls quickly through the skull to the stress-free outer surface of the head, again a consequence of the relative rigidity of the skull. For clarity we have omitted this from the figure since such a large change makes the stress distribution through the brain less clear.

The total stress at the ventricle wall is equal and opposite to the fluid pressure at this point. Since the solid parenchyma is untethered at the ventricle wall (4.3), it is the pressure in the fluid alone that induces the compression of the brain. In contrast to this, the magnitude of the total stress at the outer edge of the parenchyma is much greater than the fluid pressure and the stress there is largely due to the skull constraining the brain.

6.1.3. *Effects on the brain*

Most of the damage to the tissue of the brain, and hence most of the symptoms of hydrocephalus, occur as the result of a combination of oedema and shear stresses in the solid. The increment of fluid content may be regarded as a measure of the former, see figure 2(*e*). Notice how the increase in fluid content is largely confined to the white matter and is most pronounced in the regions adjacent to the ventricle wall. This is in agreement with the clinical observations of oedema in hydrocephalus. In the areas of grey matter close the the subarachnoid space ζ becomes negative, indicating that, in this region, fluid has been squeezed out of the brain. Given that most of the compression of the parenchyma occurs in this region, this seems to be reasonable behaviour, and is supported by clinical evidence from CT scans of hydrocephalic patients (Kaczmarek *et al.* 1997).

Note that since we have assumed that the brain is almost completely saturated with fluid, hence $\alpha = 1$ and $\beta = 0.99$, we have from (2.6) that the increment of fluid content, $\zeta(r)$, is approximately the same as the dilation, $\varepsilon(r)$. This indicates that close to the

https://doi.org/10.1017/S0022112005005707 Published online by Cambridge University Press

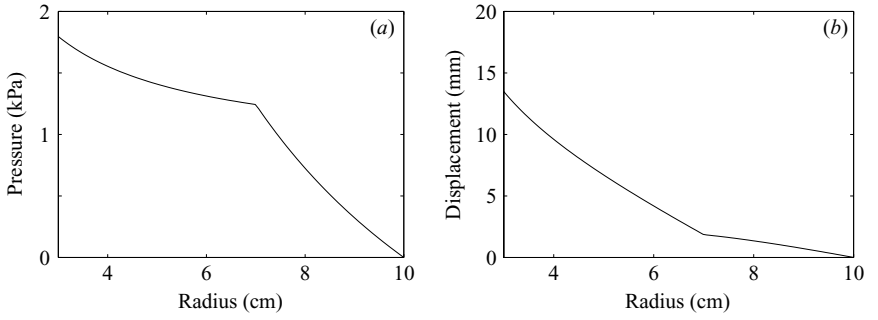


FIGURE 3. Complete occlusion: calculated values in parenchyma of (*a*) fluid pressure relative to subarachnoid pressure, (*b*) displacement when grey matter permeability decreased and stiffness increased.

ventricles the solid matrix expands, while in the peripheral regions it is compressed against the skull.

The magnitudes of the shear stresses are plotted in figure 2(*e*). This shows that in our model, the most significant tissue damage takes place in the white matter adjacent to the ventricles, a similar result to that obtained by Levine (1999).

6.2. *Effect of white–grey matter difference*

One aspect to which the model can be applied is the effect of different hydroelastic properties between white and grey matter. In general terms, if the permeability of the grey matter is decreased, then the ventricle displacement and transparenchymal pressure difference quickly increase to unphysiological values. If the stiffness of the grey matter is simultaneously increased then ventricle displacement does return to physiological values, but the pressure drop remains unacceptably high. As an example, the paramter values $k_g = 1.4^{-16}\,\mathrm{m}^2$ and $E_g = 9010\,\mathrm{Pa}$ lead to pressure in the ventricles of around 13 kPa. If the grey matter permeability is decreased by one order of magnitude, to $k_g = 1.4 \times 10^{-15}\,\mathrm{m}^2$, and $E_g = 9010\,\mathrm{Pa}$, then the pressure (higher) and ventricle displacement (lower), are still in the physiological range and this is illustrated in figure 3 for complete occlusion of the aqueduct.

6.3. *Onset of hydrocephalus*

The model allows simulation of some of the causes of hydrocephalus by varying physical parameters. First, we consider the effect of stenosis of the aqueduct, the most frequent cause of the condition, by reducing the value of d. As a second example, we model impaired absorption in the subdural space by increasing R.

6.3.1. *Stenosis of the aqueduct*

The dependence of the intraventricular pressure and ventricle wall displacement on the width of the aqueduct is shown in figure 4 where we have also shown in figure 4(*a*) the Poisseuille flow pressure drop if a flow Q_p moves through a tube of diameter d. That the pressure does not rise to Poiseuille flow level as d becomes small, indicates how much of the CSF is diverted from the aqueduct to flow through the parenchyma. It is evident that the system is resistant to even a relatively large decrease in d with little discernible effect so long as $d > 0.8\,\mathrm{mm}$, a fifth of its physiological value. Once d drops below that value, the effect on the brain is pronounced, with an increase in intraventricular pressure, $p_w(A)$, and wall displacement, $u_w(A)$ as the effective aqueduct diameter, d, approaches zero. The pressure and the displacement

https://doi.org/10.1017/S0022112005005707 Published online by Cambridge University Press

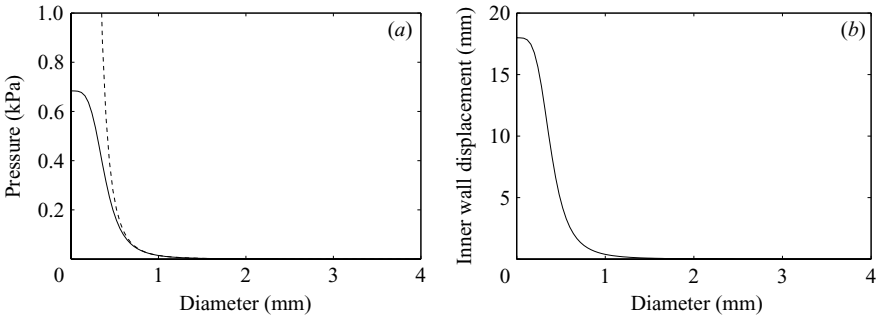


FIGURE 4. Effect of varying the aqueduct diameter, d, on pressure drop across the parenchyma and wall displacement. (a) —, pressure drop, $p_g(C) - p_w(A)$; - - -, Poiseuille pressure drop for CSF flow through tube of diameter d, (b) inner wall displacement, $u_w(A)$.

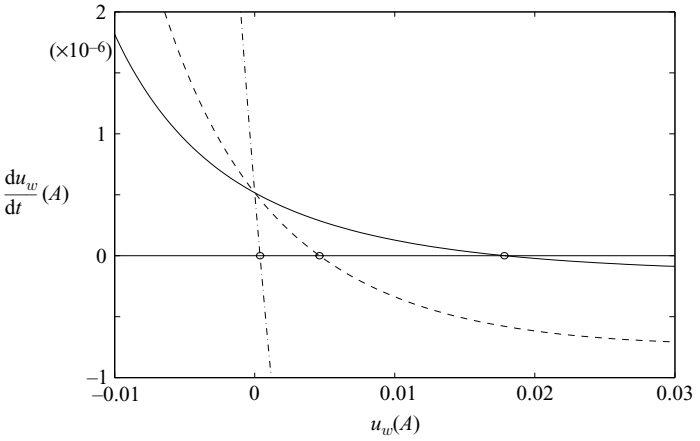


FIGURE 5. Phase plots for the wall displacement, $u_w(A, t)$ showing a stable fixed point (encircled) for various aqueduct diameter: $d = 0$ (——), $d = 0.0005$ (- - -), $d = 0.001$ (- · -).

tend to the equilibrium values determined for complete blockage of the aqueduct. The sensitivity of the model to changes in the diameter of the aqueduct below 0.8 mm is a result of the d^4 term in the Poiseuille flow pressure drop that appears in boundary conditions (4.1) and (4.10). This reinforces the view that complete occlusion of the cerebral aqueduct is the main cause of hydrocephalus.

We may model the effect of aqueduct stenosis on the time evolution of the system using the ventricular pressure boundary condition (4.1). In particular, the stability of steady-state solutions is illustrated in figure 5 by a phase plane diagram of $u_w(A)$ against $\mathrm{d}u_w(A)/\mathrm{d}t$ for a range of values of d. The phase diagram is shown for three cases; complete occlusion of the aqueduct, $d = 0$ mm, major occlusion of the aqueduct, $d = 0.5$ mm, and minor occlusion of the aqueduct, $d = 1$ mm. The steady state for the complete obstruction of the aqueduct is located at $u_w(A) = 18$ mm, corresponding to the deformation state described in the previous section, while for the open aqueduct, the steady state is located at the origin, corresponding to the undeformed configuration of the brain (the phase plot for $d = 4$ mm, its physiological value, is very similar to that for $d = 1$ mm, only with an even steeper gradient). When $d = 0.5$ mm, the deformation state is located between these two extremes.

https://doi.org/10.1017/S0022112005005707 Published online by Cambridge University Press

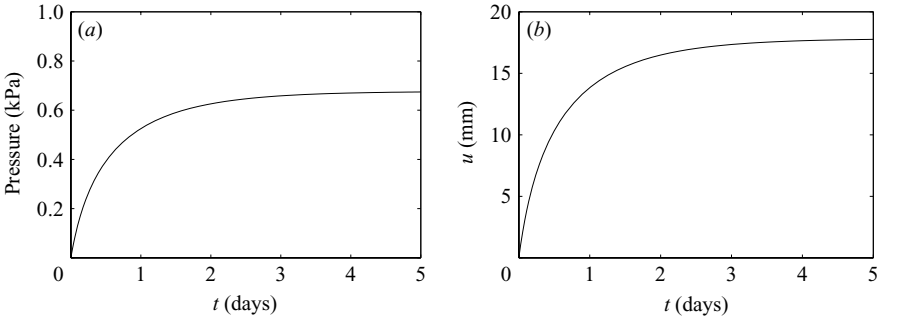


FIGURE 6. Time evolution of (*a*) the trans-paranchymal pressure drop, $p_w(A,t) - p_g(C,t)$, and (*b*) wall displacement, $u_w(A,t)$ to severe hydrocephalus following a sudden blockage of the aqueduct.

All of the steady states are stable in nature. This has important consequence for the behaviour of the brain in both healthy and pathological conditions. In the healthy state, the ventricles will return to their undeformed configuration (that is $u_w(A) = 0$) even if they are instantaneously subject to a large deformation, due to a blow to the head for example. In the pathological state, the ventricles will return to a deformed configuration even if their volume is temporarily reduced by treatment. Unless either d can be increased (by surgery to remove a tumour, for example) or a permanent alternative drainage pathway can be constructed (for example by shunting) fluid will continue to be driven through the parenchyma with the consequent rise in intraventricular pressure and deformation of the brain.

The relatively steep gradient of the phase plot in the case of the open aqueduct indicates that the brain will quickly return to steady state after being perturbed, while the shallower gradients when d is small mean that these configurations will recover more slowly.

The time evolution of hydrocephalus can be calculated by solving the differential equation for the deformation of the ventricles (4.2) numerically, the results are shown in figure 6. In formulating these solutions, we assumed that the aqueduct was suddenly completely blocked and used the initial condition $u_w(A, 0) = 0$, that is the brain is initially in its undeformed state. Both the displacement of the ventricles and the intraventricular pressure approach their steady-state values asymptotically. The time scale over which the onset of hydrocephalus occurs, approximately three days, is within the range of 'days and weeks' given by Hakim *et al.* (1976) as typical for the development of the condition. The sudden application of a blockage is also the most severe situation possible; we would expect that a blockage of the aqueduct would occur slowly and so the evolution time would be correspondingly longer.

6.3.2. *Impaired absorption of CSF*

We now consider a potential alternative to stenosis of the aqueduct as a cause of hydrocephalus. This is impaired absorption of fluid in the subarachnoid space, which in our model should correspond to an increase in R, the resitivity of the arachnoid villi. Figure 7 shows the effect on the ventricular and subarachnoid pressure of increasing R by up to around twice the value estimated from experiments. Both the ventricular and subarachnoid pressure show a linear dependence on the resistance, but the change in the magnitude of the transparenchymal pressure is negligible, so that the deformation of the ventricle also shows a negligible variation as the resistance R

https://doi.org/10.1017/S0022112005005707 Published online by Cambridge University Press

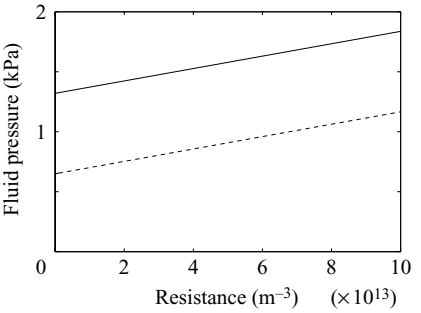


FIGURE 7. Effects of increasing the absorption resistance, R, on the ventricular pressure, $p_w(A)$, and subarachnoid pressure, $p_g(C)$.

changes. Thus, according to this model, an increase in the resistance of the arachnoid villi will not change hydrocephalic damage to the brain tissue, although the rise in fluid pressure throughout the brain may have other detrimental effects.

6.4. *Treatments*

Finally, we model some of the treatments used in cases of hydrocephalus. The most effective, and hence the most widely used, treatment is shunting and so we shall consider it in some detail, but we begin with lumbar puncture.

6.4.1. *Lumbar puncture*

In lumbar puncture, some volume of CSF is removed from the patient, usually via the spinal cord, in order to relieve fluid pressure in the skull. In terms of our model, we regard this as a step decrease in the intraventricular pressure, and hence in the displacement of the ventricle wall, without any permanent change in any of the material parameters. Clinically such a procedure has not proved to be successful in the long term, and is generally used only in severe cases where an immediate reduction of CSF pressure is required or in conjunction with another procedure such as shunting. The time-dependent version of the model would appear to explain these observations; since all of the hydrocephalic steady states are stable (see figure 5) any perturbation in $u_w(A)$ or $p_w(A)$ that is not accompanied by some change in the underlying material parameters will eventually decay, and $u_w(A)$ and $p_w(A)$ will eventually return to their steady-state pathological values. We do not include a plot of this behaviour since it would have a form the same as figure 6, which shows the pressure and deformation moving to equilibrium.

6.4.2. *Shunting*

Shunt insertion is a major surgical procedure that entails implanting a tube with a valve leading from the ventricles into some point in the body, normally an artery of the abdomen, where CSF is allowed to drain into the bloodstream. The intention of such a procedure is to create an alternative pathway for CSF drainage, and hence to relieve hydrocephalus. In addition to the difficulties normally associated with surgery on the brain, there is the question of how much fluid to drain and how to control the rate of drainage, too much can lead to the collapse of the ventricles, so-called 'slit ventricle syndrome', while too little will be insufficient to cure the illness. The main types of shunt currently used are ball-on-spring valves and silicone diaphragm valves that we model using (2.11) and (2.12), respectively. Note that in all cases in this

https://doi.org/10.1017/S0022112005005707 Published online by Cambridge University Press

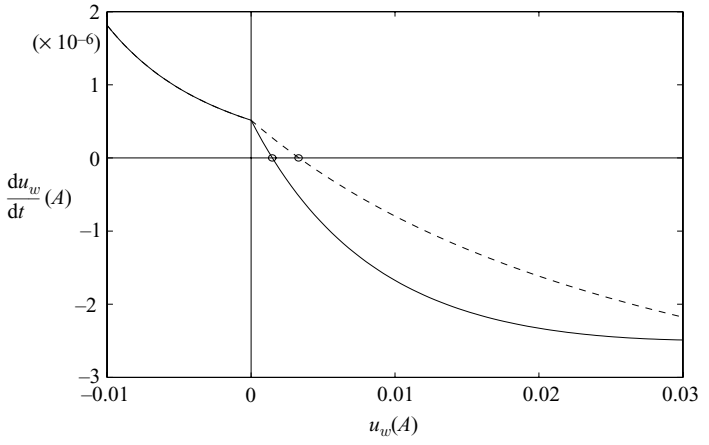


FIGURE 8. Phase plots of the ventricular wall displacement, $u_w(A)$ with shunting showing a stable fixed point for ball on spring shunt (—) and for silicone diaphragm shunt (- - -).

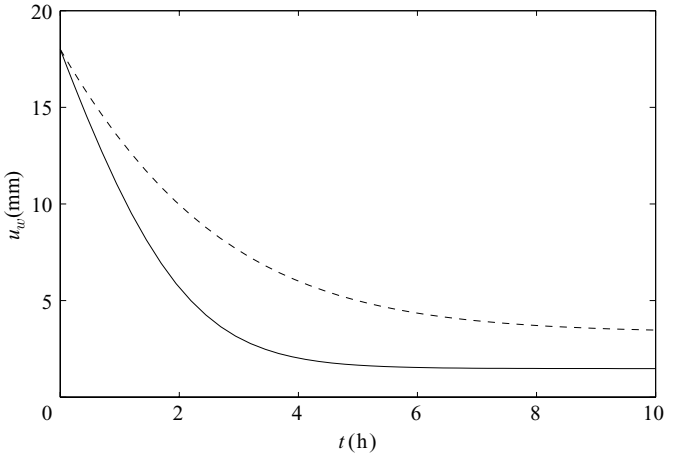


FIGURE 9. Time evolution of displacement, $u_w(A, t)$ following introduction of shunt (*a*) (—) ball on spring shunt, (*b*) (- - -) silicone diaphragm shunt.

section, we consider the case of severe hydrocephalus where the aqueduct is blocked and $d = 0$.

Phase plots of the behaviour of the ventricle wall with shunt inserted are shown in figure 8, corresponding to a ball-on-spring shunt (linear pressure–flow relationship) and to a silicone diaphragm shunt (quadratic pressure–flow relationship). In each case there is a stable steady state close to $u_w(A) = 0$, indicating that shunting may be expected to be successful in reducing the deformation and returning the ventricles to their physiological size.

The time scale for the shunts to take effect is similar, although the silicone diaphragm shunt does take a little longer, but both act over a time scale of a few hours. If the time scale for shunting to be effective is of the order of several hours, that would explain why lumbar puncture is often used in conjunction with shunting in the treatment of hydrocephalus; the lumbar puncture quickly returns the ventricles to their undeformed configuration while the shunt prevents the intraventricular pressure from rising, hence maintaining the brain in an undeformed state.

https://doi.org/10.1017/S0022112005005707 Published online by Cambridge University Press

7. Conclusions

The three main areas in which we have made significant refinements to existing models are: the specification of an appropriate set of boundary conditions for the model system, a review of the parameters to be used in describing the poroelastic properties of the brain tissue and a quasi-steady model for the time-dependent behaviour of the system that gives the evolution of hydrocephalus or the evolution of clinical treatment.

An important step forward in modelling the anatomy of the brain comes with our inclusion of the cerebral aqueduct flow in addition to poroelastic flow through the parenchyma. This enables us to simulate the behaviour of the brain and CSF pathways in their normal, non-pathological state.

A two-layered structure of the brain is useful since we can incorporate the differing material properties of the white and grey matter, though owing to a lack of experimental data we are limited in prescribing different values. Our approach here is essentially similar to that of Taylor & Miller (2004) whose parameter values lead to pressure and displacement within a physiologically acceptable range.

While the subarachnoid space is idealized as an infinitely thin layer, the boundary conditions for the subarachnoid space are more sophisticated than in existing models, where the authors have simply taken the fluid pressure to be fixed and the solid to either rigid (Nagashima *et al.* 1987; Kaczmarek *et al.* 1997; Levine 1999) or unconstrained (Tenti *et al.* 1998). Our boundary conditions enable us to consider better the effects of a change in parameters such as resistivity of the arachnoid villi or the viscosity of the CSF and to model the deformation induced in the skull. For material parameters corresponding to an adult skull, the resultant skull displacement is very small, so, in some sense, our boundary conditions are similar to those of a perfectly rigid outer layer of tissue. However, if values were known for the material properties of an infant's skull, our model could be used to analyse the magnitude of expected deformation due to congenital hydrocephalus and the effect of treatments such as compressive head wrapping.

We have considered the question of which values to use for the material parameters that appear in the governing equations. In particular, we use what we believe to be suitable values for the Young's modulus and Poisson's ratio of the white and grey matter. We also estimate values for the Reynolds number for flow in the aqueduct.

The mathematical analysis of the development and treatment of hydrocephalus that we performed has not been attempted previously, we therefore believe that such an analysis represents a significant step towards a model of the illness that is both physically realistic and clinically useful. Our results for the onset of hydrocephalus due to stenosis of the aqueduct appear to be in agreement with clinical observations, both in terms of the stability of the hydrocephalic steady state and the time scale for its development.

Our results for the effect of shunting appear to be of some relevance, indicating the effectiveness of shunting in reducing the intraventricular pressure which is the cause of hydrocephalus. Since our model of shunting is somewhat crude, it is the qualitative nature of these results, rather than the precise values for the location of the steady states that arise and the time scale for the relief of the condition, that we believe to be of most interest.

There are a number of extensions to this model that need to be considered. The very simple spherical geometry could be enhanced by using more sophisticated numerical

https://doi.org/10.1017/S0022112005005707 Published online by Cambridge University Press

solutions. Taylor & Miller (2004) have begun to use finite-element solutions, albeit in two-dimensional geometry and there is a need for both geometrically accurate models and broader geometrically simplified models such as those presented here. Levine (1999) proposed a refinement to the governing equation for the fluid so that it includes the effect of trans-parenchymal absorption of CSF, where some fluid is absorbed by capillaries in the brain before it reaches the subarachnoid space. This leads to a new term in (3.2) and (3.3), which results in solutions in the form of hyperbolic sine and cosine functions. It may also be possible to incorporate the variable permeability model of Klachnar & Tarbell (1987) where again full numerical solutions would be necessary, but as we have pointed out, such a vital extension requires better knowledge of the physical characteristics of the parenchyma. Since brain tissue is unlikely to display a linear stress–strain response, nonlinear elastic theory, especially hyperelasticity, which has been applied with some success in other areas of biomechanics (Humphrey 2003), may be a way of formulating a more accurate constitutive relationship for the white and grey matter. Incorporating the porous nature of brain tissue into this type of nonlinear theory is likely to present a mathematically challenging problem that, if resolved, may have a wide range of applications in biomechanics.

We have presented a model for the development of hydrocephalus which is, in essence, a mechanical model based on flow through the parenchyma coupled to an elevated pressure difference between the ventricles and the subarachnoid space. This is not a universally agreed mechanism. Some authors report that no transmantle pressure gradient exists (Stephensen, Tisell & Wikkelsö 2002), others do report such an effect (Hoff & Barber 1974; Connor, Foley & Balck 1984). Stephensen *et al.* (2000, p. 769) note that they have not measured the transmantle pressure during development of hydrocephalus. It is difficult to understand how a model can explain the deformation of the ventricles without a pressure gradient being present at some point and a number of authors (see the comments to Stephensen *et al.* 2002) have suggested that a pressure gradient develops in acute hydrocephalus, then dissipates gradually as the mechanical properties of the brain change. In mathematical terms, this would correspond to time-dependence in the mechanical properties of the parenchyma. This could go some way to explaining normal pressure hydrocephalus, with the brain being initially subject to pressure gradient and resulting deformation, followed by a gradual change in the material properties of the tissue which yields less resistance to CSF flow, lowering the pressure difference, without a corresponding contraction of the ventricles. However, it should be kept in mind that some mechanisms for the onset of hydrocephalus will be more subtle and complicated than the mechanical mechanism described here.

The linear and quadratic models used for ball-on-spring and silicone diaphragm shunts, respectively, are purely phenomenological in nature and the line-fitting method of parameter estimation is likely to be approximate at best. This means that our results regarding the brain deformation and time scale for the effectiveness of shunting may need to be re-evaluated, but the qualitative nature of our findings should still be correct. We chose to use this approach since the only existing mathematical models of shunting in the literature (Buchheit *et al.* 1982; Portnoy 1982) are of an elementary form. A pressure–flow relationship $S = S(\Delta p)$, based on a study of the hydrodynamic properties of shunts and validated experimentally, would therefore be of great use in the modelling of the treatment of hydrocephalus.

https://doi.org/10.1017/S0022112005005707 Published online by Cambridge University Press

REFERENCES

Albeck, M., Borgesen, S., Gjerris, F., Schmidt, J. & Sorensen, P. 1991 Intracranial pressure and cerebrospinal fluid outflow conductance in healthy subjects. *J. Neurosurg.* **74**, 597–600.

Bickers, D. & Adams, R. 1949 Hereditary stenosis of the aqueduct of sylvius as a cause of congenital hydrocephalus. *Brain* **72**, 246–262.

Biot, M. 1941 General theory of three dimensional consolidation. *J. Appl. Phys.* **12**, 55–164.

Bloomfield, I., Johnston, I. & Bilston, L. 1998 Effects of proteins, blood cells and glucose on the viscosity of cerebrospinal fluid. *Pediat. Neurosurg.* **28**, 246–251.

Bradbury, M. 1993 Anatomy and physiology of CSF. In *Hydrocephalus* (ed. P. Schurr & C. Polkey), pp. 19–47. Oxford University Press.

Buchheit, F., Maitrot, D., Healy, J. & Gusmao, S. 1982 How to choose the best valve. In *Shunts and Problems in Shunts* (ed. M. Choux), pp. 184–187. Karger, Basel.

Connor, E., Foley, L. & Balck, P. 1984 Experimental normal-pressure hydrocephalus is accompanied by increased transmantle pressure. *J. Neurosurgery* **61**, 322–327.

Czosnyka, M., Czosnyka, Z., Whithouse, H. & Pickard, J. 1997 Hydrodynamic properties of hydrocephalus shunts: UK shunt evaluation laboratory. *J. Neurol. Neurosurg. Psychiat.* **62**, 43–50.

Drake, J., Kestle, J. & Milner, R. 1998 Randomized clinical trials of cerbrospinal fluid shunt design in pediatric hydrocephalus. *Neurosurgery* **43**, 294–305.

Drake, J. & Sainte-Rose, C. 1995 *The Shunt Book*. Blackwell.

Drossos, A., Santomaa, V. & Kuster, N. 2000 The dependence of electromagnetic energy absorbtion upon human head tissue composition in the range 300–3000 MHz. *IEEE Trans. Microwave Theor. Tech.* **48**, 1988–1995.

Fay, J. 1994 *Introduction to Fluid Mechanics*. MIT Press.

Fung, Y. C. 1993 *Biomechanics: Mechanical Properties of Living Tissues*. Springer.

Hakim, S., Venegas, J.-G. & Burton, J. 1976 The physics of the cranial cavity, hydrocephalus, and normal pressure hydrocephalus: mechanical interpretation and mathmatical model. *Surgic. Neurol.* **5**, 187–210.

Hoff, J. & Barber, R. 1974 Transcerebral mantle pressure in normal pressure hydrocephalus. *Arch. Neurol.* **26**, 120–120.

Holbourn, A. 1943 Mechanics of head injuries. *Lancet* **2**, 403–410.

Humphrey, J. 2003 Continuum biomechanics of soft biological tissues. *Proc. R. Soc. Lond.* A **459**, 3–46.

Kaczmarek, M., Subramaniam, R. & Neff, S. 1997 The hydromechanics of hydrocephalus: steady state solution for cylindrical geometry. *Bull. Math. Biol.* **59**, 295–323.

Klachnar, M. & Tarbell, J. 1987 Modelling water flow through arterial tissue. *Bull. Math. Biol.* **49**, 651–669.

Kyriacou, S., Mohamed, A., Miller, K. & Neff, S. 2002 Brain mechanics for neurosurgery: modeling issues. *Biomech. Mod. Mechanobiol.* **1**, 151–164.

Lakes, R. 1993 Materials with structural hierarchy. *Nature* **361**, 511–515.

Lakes, R. 2002 Making and characterizing negative Poisson's ratio material. *Intl J. Mech. Engng Educ.* **30**, 50–58.

Levine, D. 1999 The pathogenesis of normal pressure hydrocephalus. *Bull. Math. Biol.* **61**, 875–916.

Metz, H., McElhaney, J. & Ommaya, A. 1970 A comparison of the elasticity of live, dead and fixed brain tissue. *J. Biomech.* **3**, 453–458.

Miller, K. 1999 Constitutive model of brain tissue for finite element analysis of surgical procedures. *J. Biomech.* **32**, 475–479.

Miller, K. & Chinzei, K. 1997 Constitutive modelling of brain tissue: experiment and theory. *J. Biomech.* **30**, 115–1121.

Nagashima, T., Tamaki, N., Matsumoto, S., Horwitz, B. & Seguchi, Y. 1987 Biomechanics of hydrocephalus: a new theoretical model. *Neurosurgery* **21**, 898–904.

Nolte, J. 2002 *The Human Brain: An Introduction to its Functional Anatomy*. Mosby, St Louis.

Portnoy, H. 1982 Hydrodynamics of shunts. In *Shunts and Problems in Shunts* (ed. M. Choux), pp. 179–183. Karger, Basel.

Reulen, H., Graham, R., Spatz, M. & Klatzo, I. 1977 Role of pressure gradients and bulk flow in the dynamics of vasogenic brain edema. *J. Neurosurg.* **46**, 24–35.

https://doi.org/10.1017/S0022112005005707 Published online by Cambridge University Press

van Rietbergen, H., Weinars, B., Huiskes, R. & Odgaard, A. 1995 A new method to determine bone elastic properties and loading using micromechanical finite element models. *J. Biomech.* **28**, 69–81.

Sahay, K. & Kothiyal, K. 1984 A nonlinear hyperelastic model of the pressure volume function of cranial components. *Intl J. Neurosci.* **23**, 301–309.

Sahay, K., Mehrotra, R., Sachdeva, U. & Banerji, A. 1992 Elastomechanical characterization of brain tissues. *J. Biomech.* **25**, 319–326.

Sahay, K. B. 1984 On the choice of strain energy function for mechanical characterisation of soft biological tissues. *Engng Med.* **13**, 11–14.

Sivaloganathan, S., Drake, J. & Tenti, G. 1998 Mathematical pressure volume models of the cerebrospinal fluid. *Appl. Maths Comput.* **94**, 243–266.

Smillie, A. 2003 A biomechanical model of the pathogenesis and treatment of hydrocephalus. Master's thesis, Oxford University.

Stastna, M., Tenti, G., Sivaloganathan, S. & Drake, J. 1998 Brain biomechanics: consolidation theory of hydrocephalus. Variable permeability and transient effects. *Can. Appl. Maths Q.* **7**, 93–110.

Stephensen, H., Tisell, M. & Wikkelsö, C. 2002 There is no transmantle pressure gradient in communicating or noncommunicating hydrocephalus. *Neurosurgery* **50**, 763–773.

Taylor, Z. & Miller, K. 2004 Reassessment of brain elasticity for analysis of biomechanisms of hydrocephalus. *J. Biomech.* **37**, 1263–1269.

Tenti, G., Drake, J. & Sivaloganathan, S. 2000 Brain biomechanics: mathematical modelling of hydrocephalus. *Neurolog. Res.* **22**, 19–24.

Tenti, G., Sivaloganathan, S. & Drake, J. 1998 Brain biomechanics: steady-state consolodation theory of hydrocephalus. *Can. Appl. Maths Q* **7**, 111–125.

Wang, H. 2002 *Theory of Linear Poroelasticity: with Applications to Geomechanics and Hyrdogeology*. Princeton University Press.

Weller, R., Kida, S. & Harding, B. 1993 Aetiology and pathology of hydrocephalus. In *Hydrocephalus* (ed. P. Schurr & C. Polkey), pp. 48–99. Oxford University Press.

https://doi.org/10.1017/S0022112005005707 Published online by Cambridge University Press